





Robust Gain-Tuning of the Primary Control for AC Islanded Microgrids Using an LMI-Based P-LPV/ H_{∞} Control Structure and PCA Algorithm

Fatemeh Zare-Mirakabad | Mohammad-Hosein Kazemi 🕞 | Aref Doroudi 👨

Department of Electrical Engineering, Shahed University, Tehran, Iran

Correspondence: Mohammad-Hosein Kazemi (kazemi@shahed.ac.ir)

Received: 27 July 2024 | Accepted: 25 September 2025

Funding: The authors received no specific funding for this work.

ABSTRACT

To address the issue of frequency regulation in AC-islanded microgrids (MGs), this paper introduces a novel approach for adjusting primary controller gains for AC-islanded MGs. The proposed approach uses the linear matrix inequality (LMI) for polytopic linear parameter varying (P-LPV) modelling based on the H_{∞} control theory and principal component analysis (PCA) algorithm. The objective is to regulate the MG frequency while considering the nonlinearity and uncertainty of the system. To achieve optimal control gains, the method considers all the system uncertainties in a P-LPV modelling of the system. The PCA algorithm reduces the scheduling parameter region, and the optimal control gains are computed by solving the relevant LMIs defined on the obtained P-LPV model based on H_{∞} performance and stability achievement. The primary control gains are optimised to minimise the errors between the optimal and actual control signals. Importantly, the suggested method preserves the order and structure of the primary control, making it applicable to implement on digital hardware devices. In addition, the MG is simulated in MATLAB/Simulink, and the simulation results demonstrate the authenticity, effectiveness, and efficiency of the proposed process for MG frequency regulation in the presence of uncertainties, disturbances, nonlinearity, and dynamic changes in MGs.

1 | Introduction

The rising popularity of microgrids (MGs) can be attributed to economic incentives, the growth of renewable energy sources, and increasing environmental awareness. MGs have a significant impact on enhancing power flexibility, mitigating climate change concerns, minimising energy losses, and reducing strain on transmission lines. Additionally, they efficiently integrate distributed generators (DGs) into the current energy infrastructure [1–3]. An MG constitutes a localised, active power distribution network, typically functioning at low voltage thresholds. It encompasses an array of distributed inverter-based resources, local loads, and energy storage systems. It operates as a controllable network under the monitoring of a control system. MGs may operate

in two modes: grid-connected and islanded modes. In the grid-connected mode, voltage and frequency regulation depend on the utility grid operation. As a result, the controllers are responsible for managing the active and reactive output powers of DGs. In islanded mode, the MG is disconnected from the utility grid and operates autonomously. Consequently, the controllers are responsible for regulating frequency and voltage, as well as proportional active and reactive power sharing, to ensure proper functioning [4, 5]. Hierarchical control represents the predominant control framework in both grid-connected and islanded modes within the context of MGs. This control method is structured into primary, secondary, and tertiary levels [6]. The primary control is responsible for regulating the MG voltage and frequency in order to maintain stable proportional power-

This is an open access article under the terms of the Creative Commons Attribution-NonCommercial-NoDerivs License, which permits use and distribution in any medium, provided the original work is properly cited, the use is non-commercial and no modifications or adaptations are made.

@ 2025 The Author(s). IET Generation, Transmission & Distribution published by John Wiley & Sons Ltd on behalf of The Institution of Engineering and Technology.

sharing. The secondary control is tasked with synchronising the MG with the utility grid and compensating for any frequency and voltage deviations caused by the primary level. The tertiary control is designed to optimise the economic performance of the MG and manage the power flow between the MG and the utility grid [7–9].

In practical applications, MGs encounter challenges such as parametric uncertainty and external disturbances. Classical controllers may not always ensure stability under these conditions, whereas robust control approaches are considered one of the most effective methods to address these challenges [8, 10, 11]. The H_{∞} control method is a robust technique utilised in various systems due to its capacity to tolerate unstructured uncertainties and unknown external disturbances. This method ensures system stability in the presence of bounded external disturbances, thereby limiting their impact and emphasising system robustness in uncertain environments [12]. A literature review on the MG control topic shows that the H_{∞} control can be applied at primary and secondary control levels. Reference [13] comprehensively reviews H_{∞} robust MG control methods. In [14], a distributed robust frequency control approach is operationalised within the secondary layer, employing H_{∞} theory and pole placement constraints under the LMI framework. This methodology is designed to adjust the frequency and govern the proportional active powersharing ratio in MGs, thereby enhancing the system's stability and distribution efficiency. A distributed secondary voltage and frequency controller utilising H_{∞} theory is implemented to ensure the robust performance of the closed-loop system in the presence of disturbances and sensor attacks [15]. The faulttolerant distributed control of MG is improved by [16] using the LMI method and the mixed H_2 / H_∞ controller. Also, the computational complexity is decreased by decomposing the system dynamics into first-order subsystems. In [17], a distributed cooperative robust control technique has been developed for use in the secondary layer of an MG hierarchical control system. This technique takes into account communication link disturbances and uncertainties. Necessary conditions for stability are determined using H_{∞} consensus-based control and a set of LMIs. In [18], A robust distributed $H\infty$ consensus-based control mechanism is designed for AC MGs under communication fixed time delay. In this paper, the application of Lyapunov theory enables the determination of an upper limit for the time delay that ensures the stability of the system.

The conventional H_∞ synthesis method is associated with certain limitations, including its inherent mathematical complexity (due to changing operating conditions and consequently changing the controller output) and the necessity for a highly accurate system model. Also, the controller complexity can be a substantial challenge in real-world implementations. However, in this article, these limitations have been resolved. There is no computational complexity problem because the computational part of the proposed method is done offline, and also by using the PCA technique, the dimensions of the problem have been significantly reduced.

Most of the proposed H_{∞} controllers in the MG control topic focus on the linear dynamics of MGs and employ robust linear methodologies to address challenges related to frequency and voltage regulations. Indeed, nonlinear terms in dynamic models

are not considered, while the nature of MGs includes many nonlinear factors. Designing a controller in the presence of nonlinear factors is complex and requires much computation. Using a linear parameter varying (LPV) model is a popular method for designing robust controllers for systems with nonlinear and uncertain dynamics [19–21]. In the LPV schemes, it is assumed that the system model is linear but depends on some time-varying parameters called varying parameters. Using an LPV model, the designed controller can adjust its parameters according to the system conditions. The LPV-based controllers can improve the stability, efficiency, and reliability of the MG operation [22-24]. Polytopic approaches to describe the uncertainties of an LPV system have attracted considerable attention in the field of control systems for practical applications. Their adoption is mainly attributed to their robust performance in handling complex nonlinear dynamics. This method extends the applicability of traditional linear control strategies to a wider class of systems, thereby providing a versatile framework to ensure system stability and performance in the face of parametric variations and nonlinear behaviours. Consequently, P-LPV techniques represent a pivotal advancement in the control of complex systems, aligning with the evolving sector demands for precision, reliability, and adaptability [25-27]. The actuators' and sensors' failure detection and reconstruction in DC MGs with nonlinear loads are discussed in [28], where a sliding mode technique was employed to produce a novel robust gain-scheduling detector. Then, a polytopic quasi-LPV approach was devised to estimate component failure. In [29], the LPV loop-shaping controller was proposed for grid-following inverters to regulate their output active and reactive powers. An LPV-modelled MG designs a mixed H₂/H_m linear time-varying state feedback architecture [30]. The reference [25] examines a robust control method for frequency oscillation damping in an islanded hybrid MG. The LPV model hides the nonlinearity of the wind turbine.

In most of the previous papers that proposed LPV modelling and considered the nonlinear effects of MG as varying parameters, the number of scheduling signals is increased. This growth affects the controller design process, increasing computing complexity, conservatism, and scheduling region overbounding [31, 32]. Therefore, using a dimensionality reduction technique such as a PCA algorithm is necessary to reduce the dimension of the scheduling parameter [33, 34]. In the study presented in [35], a robust structure is proposed for the voltage and current loops of the primary control using P-LPV and H_{∞} theory to regulate the frequency and voltage of the MG. It does not preserve the traditional structure of conventional controllers, while in the method presented in this article, the structure is preserved and only the adjustment of the control gains is desired.

Motivated by the advancements and constraints discussed in prior literature, this paper introduces an innovative methodology for frequency regulation in AC-islanded MGs. The approach involves optimising the primary control gains and droop coefficients. The proposed method uses a reduced P-LPV model of an MG to design an LMI-based H_{∞} control for its frequency regulation in the presence of uncertainties, disturbances, and parameter changes. The PCA algorithm reduces the dimension of the LPV scheduling parameters to minimise the computational burden. Unlike the previous approaches that changed the primary control structure, in this paper, the architecture of the primary control

system is preserved in its original form; however, a recalibration of the gain values is undertaken. This adjustment is achieved through the resolution of an optimisation problem conducted in an offline setting, thereby refining the control strategy without necessitating alterations to the underlying control structure.

Generally, the main contributions of this paper can be summarised as follows:

Without changing the primary control structure, the primary control gains and droop coefficients of all voltage source inverters (VSIs) in the MG are adjusted such that the system has a suitable robustness against nonlinear effects, disturbances, and existing uncertainties. The efficiency of the system is increased by defining an H_{∞} performance index, and therefore the stability robustness of the system is improved. This reduces computational complexity and improves scalability.

The rest of the paper proceeds as follows: Section 2 describes the preliminaries of the P-LPV modelling of MG. Section 3 explains the reduced P-LPV model using the PCA algorithm. The proposed robust gain-tuning method is represented in Section 4. Section 5 presents the numerical simulation results. Finally, Section 6 states the conclusion.

2 | Preliminaries

2.1 | Primary Control Preliminaries

The primary control is responsible for regulating the voltage and frequency, as well as maintaining the stability of MGs. Figures 1 and 2 display a typical primary control of a VSI. The primary control comprises power, voltage, and current control loops. It employs the conventional droop control strategy to achieve proportional power-sharing in active and reactive power. The power controller outputs include a reference voltage for the voltage controller and a reference frequency for the inverter bridge. The voltage controller generates the reference current for the current controller, and ultimately, the reference voltage for the inverter bridge is obtained through the current controller. Assuming that switching ripples and high-frequency harmonics are negligible, the VSI is theoretically conceptualised as an AC source within the system model. The inductive effective impedance between the VSI and the AC bus is assumed to be high. The dynamic model of the primary control, introduced in... [36–38], can be rewritten in the form of:

$$\dot{x}_1 = -\omega_{ci}x_1 + \omega_{ci}\left[x_6x_7 + x_{11}x_{12}\right] \tag{1}$$

$$\dot{x}_2 = -\omega_{ci} x_2 + \omega_{ci} \left[-x_6 x_{12} + x_{11} x_7 \right] \tag{2}$$

$$\dot{x}_3 = -x_6 + u_1 + V_{in} \tag{3}$$

$$\dot{x}_4 = F_i x_7 - \omega_b C_{fi} x_{11} - x_5 + u_2 + K_{PVi} V_{in} \tag{4}$$

$$\dot{x}_5 = -R_{fi}x_5/L_{fi} - x_6/L_{fi} + u_3 + K_{PCi}K_{PVi}V_{in}/L_{fi}$$
 (5)

$$\dot{x}_6 = x_5 / C_{fi} - x_7 / C_{fi} + \omega_{ni} x_{11} + u_4 \tag{6}$$

$$\dot{x}_7 = -R_{ci}x_7/L_{ci} + \omega_{ni}x_{12} + x_6/L_{ci} + u_5 + d_1 \tag{7}$$

$$\dot{x}_8 = -x_{11} \tag{8}$$

$$\dot{x}_9 = F_i \ x_{12} + \omega_b C_{fi} x_6 - x_{10} + u_6 \tag{9}$$

$$\dot{x}_{10} = -R_{fi}x_{10}/L_{fi} - x_{11}/L_{fi} + u_7 \tag{10}$$

$$\dot{x}_{11} = -\omega_{ni}x_6 + x_{10}/C_{fi} - x_{12}/C_{fi} + u_8 \tag{11}$$

$$\dot{x}_{12} = -R_{ci}x_{12}/L_{ci} - \omega_{ni}x_7 + x_{11}/L_{ci} + u_9 + d_2 \tag{12}$$

where the state vector of DG_i , $x \in \mathbb{R}^{12}$, is defined as:

$$x = [x_{1} ... x_{12}]^{T}$$

$$= [P_{i} Q_{i} \phi_{di} \gamma_{di} I_{ldi} V_{odi} I_{odi} \phi_{qi} \gamma_{qi} I_{lqi} V_{oqi} I_{oqi}]^{T}$$
(13)

and $\phi_{di} := \int (V_{odi}^* - V_{odi}) dt$, $\phi_{qi} := \int (V_{oqi}^* - V_{oqi}) dt$, $\gamma_{di} := \int (I_{odi}^* - I_{odi}) dt$, $\gamma_{qi} := \int (I_{oqi}^* - I_{oqi}) dt$; $d_1 := -V_{bdi}/L_{ci}$, and $d_2 := -V_{bqi}/L_{ci}$ are considered as disturbances.

The signals u_i , i = 1, ..., 9 are considered as actual control signals according to Figure 2 which are defined as follows:

$$u_1 := -n_Q x_2 \tag{14}$$

$$u_2 := -K_{PVi}n_Qx_2 + K_{IVi}x_3 - K_{PVi}x_6 \tag{15}$$

$$u_{3} := -m_{Pi}x_{1}x_{10} - K_{PCi}K_{PVi}n_{Q}x_{2}/L_{fi} + K_{ICi}x_{4}/L_{fi}$$

$$+ K_{PCi}K_{IVi}x_{3}/L_{fi} - K_{PCi}K_{PVi}x_{6}/L_{fi}$$

$$+ K_{PCi}F_{i}x_{7}/L_{fi} - K_{PCi}\omega_{b}C_{fi}x_{11}/L_{fi}$$
(16)

$$u_4 := -m_{Pi} x_1 x_{11} \tag{17}$$

$$u_5 := -m_{p_i} x_1 x_{12} \tag{18}$$

$$u_6 := -\bar{K}_{PVi} x_{11} + \bar{K}_{IVi} x_8 \tag{19}$$

$$u_7 := m_{Pi} x_1 x_5 + \bar{K}_{PCi} \omega_b C_{fi} x_6 / L_{fi} + \bar{K}_{PCi} \bar{K}_{IVi} x_8 / L_{fi}$$
$$+ \bar{K}_{ICi} x_9 / L_{fi} - \bar{K}_{PCi} x_{10} / L_{fi} - \bar{K}_{PCi} \bar{K}_{PVi} x_{11} / L_{fi}$$
(20)

$$u_8 := m_{Pi} x_1 x_6 \tag{21}$$

$$u_9 := m_{Pi} x_1 x_7 \tag{22}$$

As can be seen, these equations are nonlinear and contain some disturbances. Moreover, operating conditions may change some parameters (I_{odi} , I_{oqi} , V_{odi} , V_{oqi} , C_{fi} , R_{fi} , L_{fi} , L_{ci} , and R_{ci}).

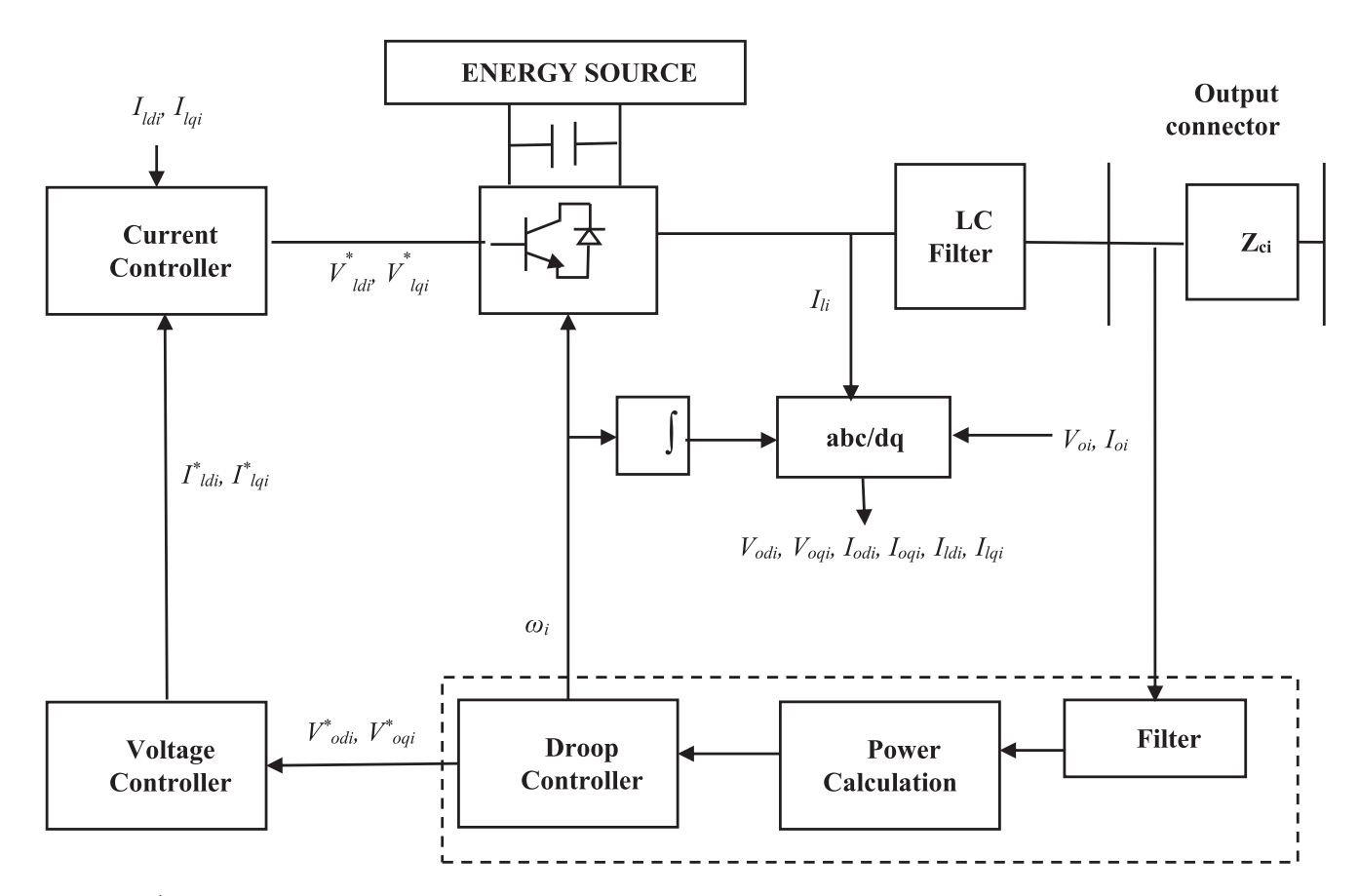


FIGURE 1 | Typical structure of primary control in MGs.

2.2 | The P-LPV Model

A popular method for controlling nonlinear systems with uncertain dynamics is the use of a P-LPV model. An P-LPV form of standard state space equation with state vector $x \in R^n$, exogenous input $w \in R^{n_w}$, control input $u \in R^{n_u}$, control objective $z_\infty \in R^{n_z}$, and the varying parameter $\mu \in R^{\bar{\mu}}$ is represented in a compact form as [39]:

$$\dot{x} = A(\mu)x + B_1(\mu)w + B_2(\mu)u z_{\infty} = C(\mu)x + D_1(\mu)w + D_2(\mu)u$$
(23)

All the matrices have appropriate dimensions and are limited to the polytope P defined as the convex hull of the finite number of matrices Q_i , called the vertices model, as:

$$Q_{i} = \begin{pmatrix} A_{i} & B_{1i} & B_{2i} \\ C_{i} & D_{1i} & D_{2i} \end{pmatrix}, i = 1, 2, \dots, N$$
 (24)

where N is the number of vertices. A convex polytopic model $Q(\mu)$ of the system can be formed as:

$$Q(\mu) = \begin{pmatrix} A(\mu) & B_1(\mu) & B_2(\mu) \\ C(\mu) & D_1(\mu) & D_2(\mu) \end{pmatrix}$$
(25)

$$Q(\mu) \in P := Co\{Q_i, i = 1, 2, ..., N\}$$

$$:= \left\{ Q(\mu) | Q(\mu) = \sum_{i=1}^{N} \alpha_i Q_i, \sum_{i=1}^{N} \alpha_i = 1, \alpha_i \ge 0 \right\}$$
 (26)

2.3 | The P-LPV Model of a VSI

In this section, the P-LPV model of a typical VSI is presented. The P-LPV model of a VSI is a mathematical representation that captures the dynamic behaviour of the inverter under various operating conditions. The model is parameterised by certain variables that can change over time or with the operating point. Hence the term 'parameter-varying'. The P-LPV model is useful for designing advanced control strategies that can adapt to changing conditions and ensure optimal performance of the VSI across its entire operating range. It's a more flexible approach compared to traditional fixed-parameter models and is particularly beneficial in applications where the system dynamics are highly nonlinear or subject to significant external disturbances.

In the context of the P-LPV model, the following variables are defined:

• Scheduling signal vector (ρ): This vector includes the parameters that the LPV model depends on. These parameters can vary over time and are known as scheduling parameters. They could represent factors like I_{odi} , I_{oqi} , V_{odi} , V_{oqi} , C_{fi} , R_{fi} , L_{fi} , L_{ci} , and R_{ci} that influence the system's dynamics.

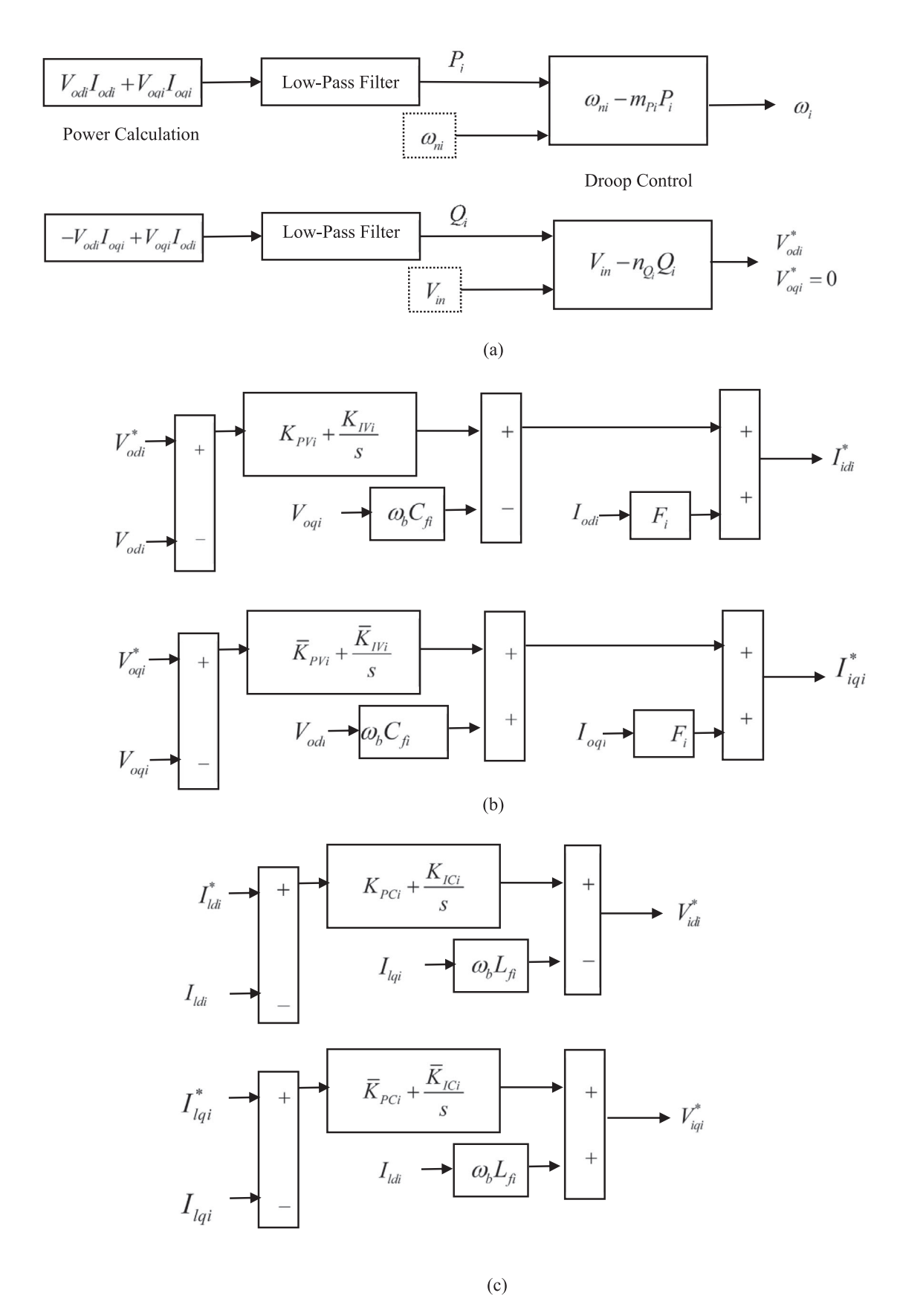


FIGURE 2 | Primary control blocks of MGs: (a) Power control, (b) Voltage control and (c) Current control.

- Exogenous input vector (w): This vector represents external inputs to the system that are not control inputs. These could include V_{in}, d₁, and d₂ affecting the VSI's performance.
- Control input vector (*u*): This is the vector of inputs that the control system can manipulate to achieve desired performance. In the case of a VSI, this could include control signals.

The vector of the scheduling signal $\rho(t) \in R^{\bar{\rho}}$, $\bar{\rho} = 9$, the exogenous input $w \in R^3$, and the control input $u \in R^9$ are defined as:

$$\rho = [\rho_1 \dots \rho_9]^T = [x_7 \ x_6 \ x_{12} \ x_{11} \ C_{fi} \ R_{fi} \ L_{fi} \ L_{ci} \ R_{ci}]^T$$

$$w = [V_{in} \ d_1 \ d_2]^T, u = [u_1 \dots u_9]^T$$
(27)

To show the VSI system Equations (1) to (12) in the form of an P-LPV model in Equation (23), the varying parameters $\mu(t) \in R^{\bar{\mu}}$, $\bar{\mu} = 10$, are defined $\mu(t) = h(\rho(t))$ as follows:

$$\begin{cases} \mu_{1} = 0.5\omega_{ci}\rho_{1}, \mu_{2} = 0.5\omega_{ci}\rho_{2}, \mu_{3} = 0.5\omega_{ci}\rho_{3}, \\ \mu_{4} = 0.5\omega_{ci}\rho_{4}, \mu_{5} = -\omega_{b}\rho_{5}, \mu_{6} = -\rho_{6}/\rho_{7}, \\ \mu_{7} = -1/\rho_{7}, \mu_{8} = -1/\rho_{9}, \mu_{9} = 1/\rho_{9}, \\ \mu_{10} = -\rho_{9}/\rho_{8}. \end{cases}$$
(28)

Hence, the LPV model of Equations (1–12) can be rewritten as:

$$\dot{x}_1 = -\omega_{ci}x_1 + \mu_1x_6 + \mu_2x_7 + \mu_3x_{11} + \mu_4x_{12} \tag{29}$$

$$\dot{x}_2 = -\omega_{ci}x_2 - \mu_3x_6 + \mu_4x_7 + \mu_1x_{11} - \mu_2x_{12} \tag{30}$$

$$\dot{x}_3 = -x_6 + u_1 \tag{31}$$

$$\dot{x}_4 = -x_5 + F_i x_7 + \mu_5 x_{11} + u_2 \tag{32}$$

$$\dot{x}_5 = \mu_6 \ x_5 + \mu_7 x_6 + u_3 \tag{33}$$

$$\dot{x}_6 = \mu_8 \ x_5 - \mu_8 x_7 + \omega_{ni} x_{11} + u_4 \tag{34}$$

$$\dot{x}_7 = \mu_9 \ x_6 + \mu_{10} x_7 + \omega_{ni} x_{12} + u_5 + d_1 \tag{35}$$

$$\dot{x}_8 = -x_{11} \tag{36}$$

$$\dot{x}_9 = -\mu_5 x_6 - x_{10} + F_i x_{12} + u_6 \tag{37}$$

$$\dot{x}_{10} = \mu_6 \ x_{10} + \mu_7 x_{11} + u_7 \tag{38}$$

$$\dot{x}_{11} = -\omega_{ni}x_6 + \mu_8x_{10} - \mu_8x_{12} + u_8 \tag{39}$$

$$\dot{x}_{12} = -\omega_{ni}x_7 + \mu_9 x_{11} + \mu_{10}x_{12} + \mu_9 + d_2 \tag{40}$$

Equations (29) to (40) can be rewritten in LPV compact form as:

$$\dot{x} = A(\mu)x + B_1w + B_2u$$

$$z_{\infty} = Cx$$
(41)

where, the matrices A, B_1 , B_2 , and C are given in Appendix A. The states x_3 , x_6 , x_7 , x_8 , x_{11} , and x_{12} , which have an important effect on the system, are considered as control objective (z_{∞}). Equation (41) shows that only the matrix A is dependent on varying parameters μ , while B_1 , B_2 , and C are constant and independent of μ .

For constructing a polytopic model, only three values for each scheduling signal are considered, and they are the minimum, middle, and maximum values of each scheduling signal interval range. In this way, $N=3^{\bar{\rho}}=3^9$ vertices are produced, which are noted by $M_i:=(A_i,B_1,B_2,C)$. Then, the polytopic model of DG_i can be expressed as:

$$P_{a} = \{ (A(\mu), B_{1}, B_{2}, C) \mid (A(\mu), B_{1}, B_{2}, C)$$

$$= \sum_{i=1}^{N} \alpha_{i} M_{i}, \sum_{i=1}^{N} \alpha_{i} = 1, \alpha_{i} \ge 0 \}$$
(42)

The matrix $A(\mu)$ is a continuous function in terms of the parameter vector $\mu(t)$, depending on the scheduling signal $\rho(t)$ according to parameter mapping (28).

3 | Reduced P-LPV Model Using PCA Algorithm

The selection of the number of vertex models, denoted as N, should be made with careful consideration of the system's operating range, nonlinearity effects, and system parameter dimensions to ensure that all dynamic behaviours of the system are adequately captured. However, it is important to note that an increase in N leads to heightened complexity in controller computations. The PCA method can be utilised to facilitate the identification of a reduced region within the parameter space [40–42]. In the context of this problem, the presence of ten parameters ($\bar{\mu} = 10$) necessitates the utilization of 2^{10} vertices in order to construct a polytopic model for the system.

Such a high number of vertices significantly increases the computational workload. Therefore, the PCA-based parameter set mapping technique is utilised to reduce the number of vertices.

In the PCA approach, and for the scheduling signal $\rho(t)$, the mapping $\eta(t)=r(\rho(t))$, where $r:R^{\bar{\rho}}\to R^{\bar{\eta}}$ and $\bar{\eta}<\bar{\mu}$, should be found such that the following reduced LPV model can be replaced by Equation (41).

$$\dot{x} = \hat{A}(\eta)x + B_1w + B_2u$$

$$z_{\infty} = C x$$
(43)

The parameters of the original polytopic model in Equation (42) for i=1,2,...,N are collected to form a $\bar{\mu}\times N$ matrix $\Theta=[\mu^1,\mu^2,...,\mu^N]$ called the data matrix, where μ^i is the parameter vector evaluated at the i^{th} vertex. The normalised form of the data matrix $\Theta^n=\prod(\Theta)$ with zero mean and unit standard deviation can be obtained by applying an affine law [40]. Then, the following singular value decomposition of Θ^n is performed.

$$\Theta^{n} = \begin{bmatrix} \hat{U} & U \end{bmatrix} \begin{bmatrix} \hat{\Sigma} & 0 \\ 0 & \Sigma \end{bmatrix} \begin{bmatrix} \hat{V}^{T} \\ V^{T} \end{bmatrix}$$
 (44)

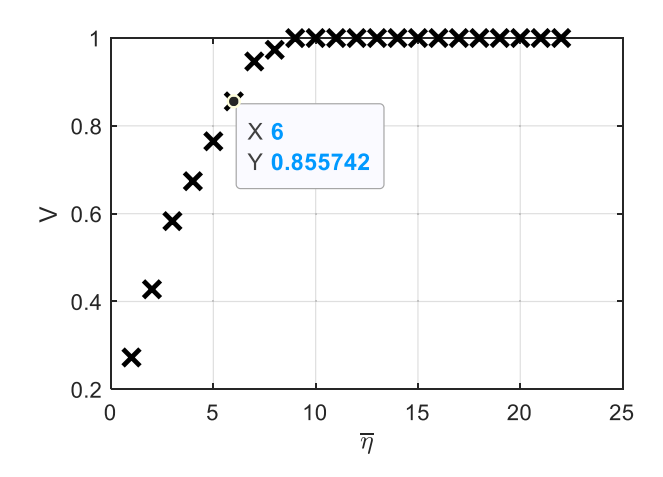


FIGURE 3 | Variations of V versus $\bar{\eta}$.

where $\hat{\Sigma}$ and Σ are diagonal submatrixes whose elements are the significant and nonsignificant singular values, respectively. By picking up the significant singular values and their associated submatrices \hat{U} , $\hat{\Sigma}$, and \hat{V} , and eliminating the nonsignificant singular values, one can write $\hat{\Theta}^n = \hat{U} \hat{\Sigma} \hat{V}^T \approx \Theta^n$, in which $\hat{\Theta}^n$ is an approximation of the normalised data matrix Θ^n . The submatrix \hat{U} is used as a basis of the significant column space to realise the reduced mapping:

$$\eta(t) = r(\rho(t)) = \hat{U}^T \Pi(h(\rho(t))) = \hat{U}^T \Pi(\mu(t))$$
 (45)

So, the approximate mapping of $\hat{A}(.)$ in Equation (43) is related to Equation (41) by the following equation:

$$\hat{A}\left(\eta\left(t\right)\right) = A\left(\hat{\mu}\left(t\right)\right)$$

$$\hat{\mu}\left(t\right) = \Pi^{-1}\left(\hat{U}\eta\left(t\right)\right) = \Pi^{-1}\left(\hat{U}\hat{U}^{T}\Pi\left(\mu\left(t\right)\right)\right)$$
(46)

where \prod^{-1} indicates the rescaling of each row. So, by using $\hat{\Theta}^n$ to make new vertices (\hat{A}_i, B_1, B_2, C) , the P-LPV model in Equation (42) can be reduced to:

$$\hat{P} = \{ (\hat{A}(\eta), B_1, B_2, C) | \hat{A}(\eta) = \sum_{i=1}^{\hat{N}} \alpha_i \hat{A}_i \}$$
 (47)

where $\sum_{i=1}^{\hat{N}} \alpha_i = 1$, $\alpha_i \geq 0$, and $\hat{N} = 2^{\bar{\eta}}$ is the number of vertices, and (\hat{A}_i, B_1, B_2, C) is the i^{th} vertex model. The following index can be used as a criterion to measure the accuracy of the approximated polytopic model in Equation (47) relative to the actual polytopic model in Equation (42):

$$V_{\bar{\eta}} = \sum_{i=1}^{\bar{\eta}} \sigma_i^2 / \sum_{i=1}^{\bar{\mu}} \sigma_i^2$$
 (48)

where σ_i is the i^{th} singular value. To choose the appropriate value for $\bar{\eta}$, Equation (48) is shown in Figure 3 for different values of $\bar{\eta}$. It can be seen in Figure 3, $\bar{\eta}=6$ is the best value regarding the desired acceptable percentage error. Consequently, the simplified polytopic model in Equation (47) will only contain $\hat{N}=2^6=64$ vertices.

4 | The Robust Gain-Tuning Method

This section uses an LMI-based P-LPV/PCA/ H_{∞} control method to adjust the primary controller gains and droop coefficients of an AC islanded MG. The proposed method includes all system uncertainties as a P-LPV framework for applying the control gains tuning approach. The PCA algorithm reduces the scheduling parameter size. The optimal control gains are computed by solving the relevant LMIs defined on the reduced P-LPV model based on the H_{∞} performance and stability index. The primary control gains and droop coefficients are chosen such that the errors between the optimal and actual control signals are minimised. In the suggested method, the order and structure of the primary control remain unchanged.

The H_{∞} performance can be achieved by synthesising a control signal $(u=K_{H\infty}\,x)$ for Equation (47), which minimises attenuation for any external input $w\in l_2[0,\infty)$. This is confirmed by $Z_{\infty}\in l_2$ and $||Z_{\infty}||_2\langle\gamma||w||_2$, where $||\cdot||_2$ is the 2-norm index, l_2 is L_2 -norm space, and $||w||_2\neq 0$. The following Lemma outlines the conditions for the optimal state-feedback controller gain matrix, $K_{H\infty}$, to stabilise the closed-loop system and demonstrate the attenuation level γ .

Lemma 1. [43–45] (The problem of suboptimal overall H_{∞} static state feedback control): If matrices $Q=Q^T>0$ and T, with appropriate dimensions, satisfy the following LMIs, then the state feedback controller gain $K_{H\infty}=TQ^{-1}$ achieves quadratic stabilisation of the P-LPV system in Equation (47) for disturbance attenuation $\gamma>0$.

$$\begin{bmatrix} \hat{A}_{i}Q + Q\hat{A}_{i}^{T} + B_{2}T + T^{T}B_{2}^{T} & * & * \\ B_{1}^{T} & -I & * \\ CQ & 0 & -\gamma^{2}I \end{bmatrix} < 0$$

$$i = 1, 2, ..., \hat{N}$$
(49)

where, the symbol * indicates symmetric blocks in the LMIs.

Using the above Lemma 1 and solving the LMIs of Equation (49), the gain of the controller $K_{H\infty}$ can be obtained. Then, the optimal control signal for each DG is realized as:

$$U_{\infty} = K_{H_{\infty}} x \tag{50}$$

The primary controller gains and droop coefficients vector is:

$$G := \left[m_{Pi}, n_{Oi}, K_{PVi}, K_{IVi}, \bar{K}_{PVi}, \bar{K}_{IVi}, K_{PCi}, K_{ICi}, \bar{K}_{PCi}, \bar{K}_{ICi} \right]$$
(51)

Defining the following relative error signals as:

$$e_j := \left(\frac{u_j}{U_{\infty_j}} - 1\right) \tag{52}$$

where $[\cdot]_j$ denotes the j^{th} element of each vector, to form the error signal (e). It should be noted that since each control signal belongs to a different variation range, relative error has been used to normalise them. For the offline computation of the error signal, which is related to both of the actual and the optimal control signals, the state variables (x), are measured at the nominal operation condition. This presumption allows for a systematic evaluation of the control system's performance

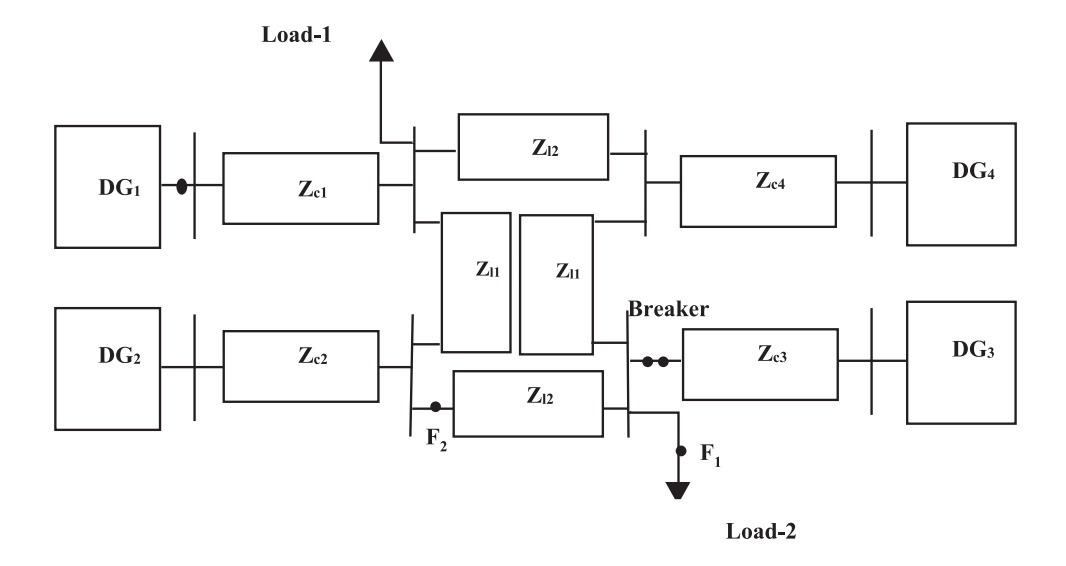


FIGURE 4 | The simulated MG.

by providing a benchmark for the deviation analysis, thereby enabling the precise adjustment of the control signals in accordance with the desired system behaviour. The relative error (e) is determined by applying Equation (53) on Equations (14) to (22), and then the optimal primary controller gains and droop coefficients are calculated by solving the following optimisation problem:

$$G^* = \underset{C}{Min} \|e\| \tag{53}$$

4.1 | Performance Improvement Discussion

By using the optimal primary control gains G^* , it is clear that error signals in Equation (52) are minimised. On the other hand, from Equation (52) it can be concluded that $u=U_{\infty}+diag\{U_{\infty}\}e$. By subsisting it at Equation (41), it results that $\tilde{d}=diag\{U_{\infty}\}e$ is added to the disturbance signal in Equation (41). So, it can be seen that by implementing the optimisation in Equation (52), you will basically impose less disturbance to the system, and this will increase the system performance.

5 | Numerical Simulation Results

This section presents the simulation results to demonstrate the effectiveness of the proposed method (PM). The AC islanded MG is simulated in MATLAB/Simulink under various scenarios, such as MG load variations, faults, plug-and-play, and parameter alterations. These simulations are critical in ascertaining both the effectiveness and the robustness of the proposed scheme. Figure 4 shows a 380 V, 50 Hz islanded MG composed of four DG units and two loads. The parameters of the simulated MG are listed in Table 1. The proposed methods are compared with the conventional method (CM) referenced in [46] and the robust method (RM) in [35] to show the better dynamic performance and efficiency of the proposed method. The conventional primary

control parameters, which are shown in Table 2, have been widely used in many studies.

According to the simulation data in the nominal case, the following ranges of variations are considered for scheduling signals.

$$\begin{cases} \rho_1 = 28 \pm 20\% \ \rho_2 = 537 \pm 10\% \\ \rho_3 = -48 \pm 35\% \ \rho_4 = 0 \pm 0.1 \\ \rho_5 = 5 \times 10^{-5} \pm 10\% \ \rho_6 = 0.1 \pm 10\% \\ \rho_7 = 1.35 \times 10^{-3} \pm 10\% \ \rho_8 = 3.5 \times 10^{-2} \pm 10\% \\ \rho_9 = 0.03 \pm 10\% \end{cases}$$
(54)

Allowing for three values of minimum, middle, and maximum for each scheduling signal yields $N=3^9$ vertices for the initial polytopic model of each DG. Applying the PCA algorithm, the reduced polytopic model in Equation (7) is achieved with $\hat{N}=2^6=64$ vertices. Finally, the primary control gains are obtained after solving LMIs in Equation (50) and the optimisation problem in Equation (54).

5.1 | Loads Change Scenario

This section demonstrates the load changes scenario to showcase the performance of the PM. At t=0 s, the MG operates in an islanded mode, and the primary control is activated simultaneously. The load changes occur at t=0.5, 1, and 1.5 s based on Table 3. In order to verify the H_{∞} performance criterion for each DG, Table 4 tabulates the performance index achievement level. Figure 5 displays the frequency, active power, and voltage output of DGs. The results indicate that the PM outperforms the CM and RM approaches. Additionally, the frequency and voltage deviations of the MG are within a stable range ($\Delta f = \pm 0.3 \ Hz$ and $\Delta V = 10\%$) [47]. Proper adjustment of the droop coefficients and other primary control gains ensures the correct regulation of MG frequency and voltage.

TABLE 1 The simulated MG parameters.

Description	DG 1&2		DG 3&4
Rating	45 kVA		34 kVA
$R_c\left(\Omega\right)$	0.03		0.03
L_{c} (mH)	0.35		0.35
Frequency (Hz)	50		50
ω	314		314
$R_f(\Omega)$	0.1		0.1
$L_f(mH)$	1.35		1.35
$C_f(\mu F)$	50		50
Description	Line 1	Line 2	Line 3
$R_{li}\left(\Omega\right)$	0.23	0.35	0.23
L_{li} (μH)	318	1847	318
Description	Load 1		Load 2
P(kW) + jQ(kVar)	(12 + j12)		(15.3 + j7.6)
Description	Parameter DG 1&2		DG 3&4
Droop coefficients	m_P	4.7×10^{-5}	6.25×10^{-5}
	n_Q	0.00065	0.00075
Voltage control gains	K_{PVi} , $ar{K}_{PVi}$	0.105	0.105
	K_{IVi} , $ar{K}_{IVi}$	441	441
Current control gains	K_{PCi} , $ar{K}_{PCi}$	15.75	15.75
	$K_{ICi},ar{K}_{ICi}$	21000	21000

 $\begin{tabular}{lll} \textbf{TABLE 2} & | & \textbf{The conventional primary control gains [46]}. \end{tabular}$

Description	Gain parameter	DG 1&2	DG 3&4
Droop coefficients	m_P	9.4×10^{-5}	12.5×10^{-5}
	n_Q	0.0013	0.0015
Voltage control gains	$K_{PVi},ar{K}_{PVi}$	0.1	0.05
	$K_{IVi},ar{K}_{IVi}$	420	390
Current control gains	$K_{PCi},ar{K}_{PCi}$	15	10.5
	$K_{ICi},ar{K}_{ICi}$	20,000	16,000

TABLE 3 | The loads change scenarios.

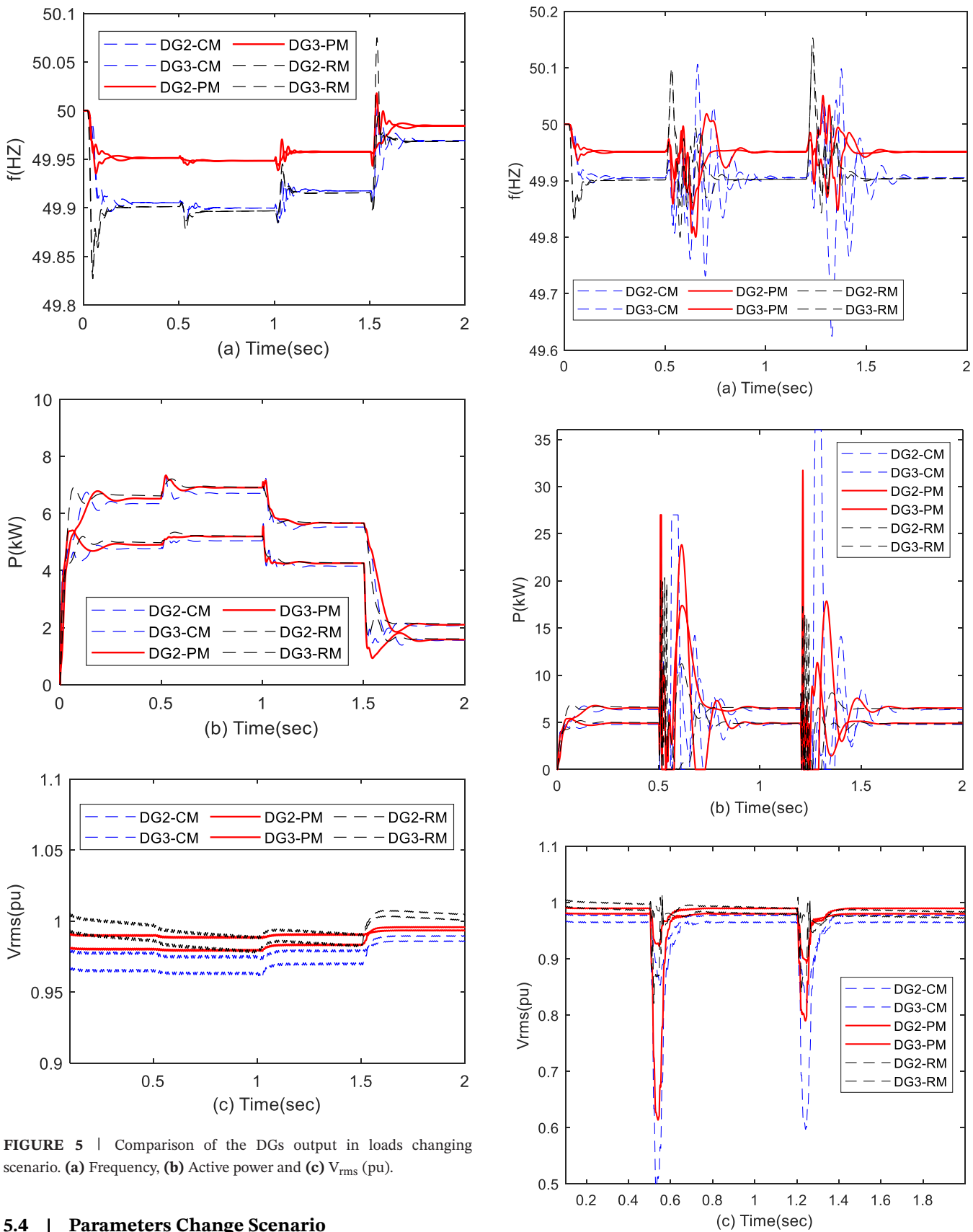
Description of scenarios	Load_1 (P(kW) + jQ (kVar))	Load_2 P(kW) + jQ (kVar)
0 < t < 0.5(s)	(12 + j12)	(15.3 + j7.6)
0.5 < t < 1(s)	$1.2 \times (12 + j12)$	(15.3 + j7.6)
1 < t < 1.5(s)	(12 + j12)	$0.8 \times (15.3 + j7.6)$
1.5 < t (s)	(12 + j12)	Disconnected

5.2 | Single Phase Fault Scenario

The following scenario tests the robustness of the PM by applying a single phase to the ground fault. A single phase-to-ground fault occurs at $t = 0.5 \, s$ and $t = 1.2 \, s$ at points F1 and F2 of the MG for a duration of 0.04 s. Additionally, Figure 6 displays the frequency, active power, and RMS voltage of DGs. The results indicate that after the short circuit, the MG recovers to its stable state, but the PM demonstrates better performance than the CM and RM approaches.

5.3 | Plug- and- Play Scenario

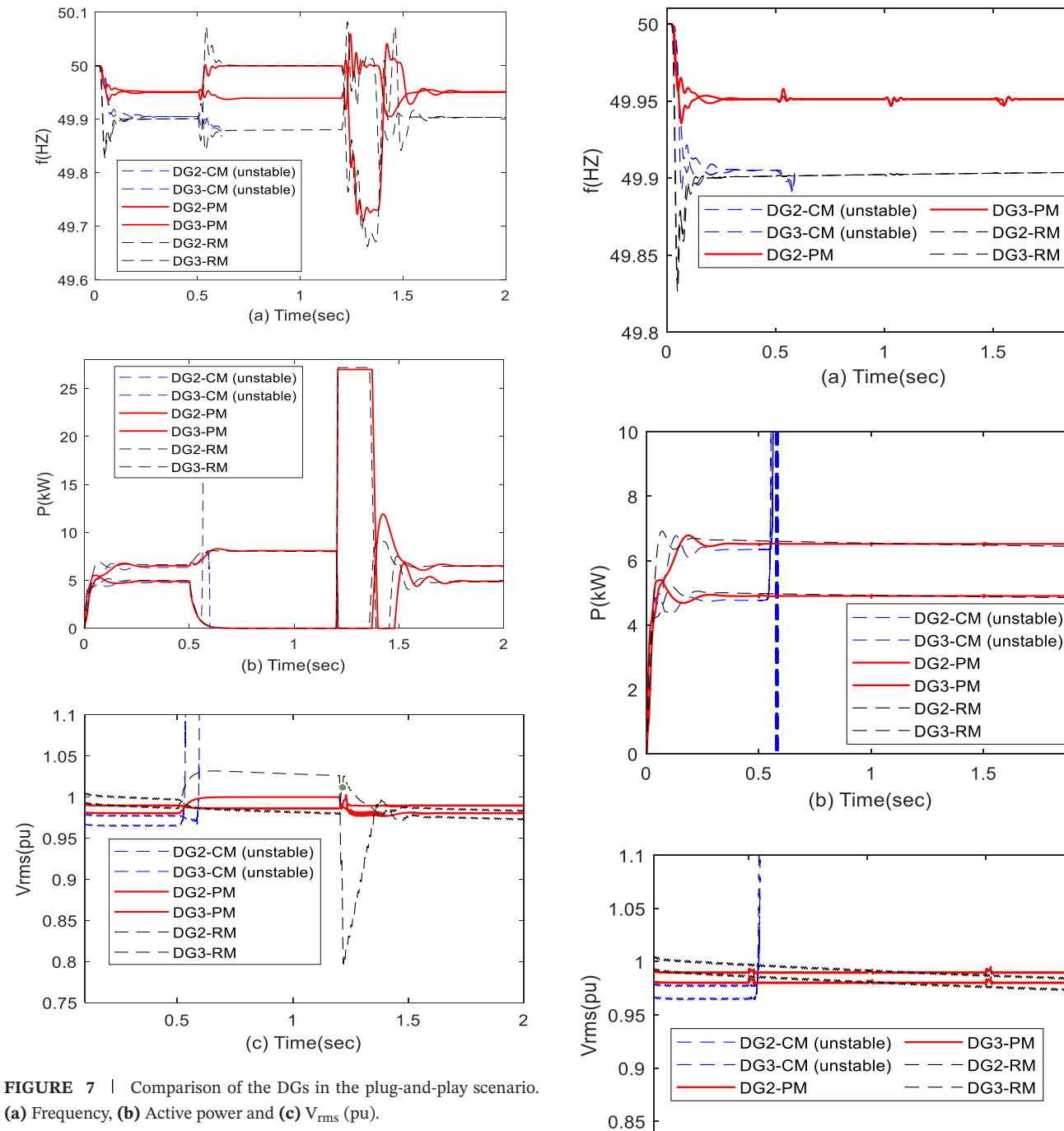
The following procedure is conducted to test the robustness of the PM in a plug-and-play scenario. At t=0 s, the MG starts operating in islanded mode with the primary control in action. At t=0.5 s, DG3 is disconnected from the MG, and at t=1.5 s, it is reconnected. Figure 7 illustrates the frequency, active power, and voltage output of the DGs. The results show that the performance of the PM is better than that of the CM and RM approaches. The frequency and voltage deviations of the MG are within the stable range. In particular, the CM approach becomes unstable, but the proposed controller prevents instability of the MG.



Parameters Change Scenario 5.4

The following section describes the scenario of parameter changes to illustrate the performance of the PM. At t = 0 s, the MG operates in an islanded mode, and the primary control is activated. The parameter changes occur at t = 0.5, 1, and 1.5 s

FIGURE 6 | Comparison of the DGs output in the case of the fault scenario. (a) Frequency, (b) Active power and (c) V_{rms} (pu).



8.0

based on Table 5. Figure 8 depicts the frequency, active power, and voltage output of DGs. The results of the PM approach are observed to be superior to the CM and RM approaches. Furthermore, the frequency and voltage deviations of MG are found to be within the stable range. The results show that the CM approach becomes unstable, while the proposed controller prevents instability of the MG. This highlights the optimal tuning of the droop coefficients and other primary control gains, which leads to the proper regulation of MG frequency and voltage.

6 Conclusion

This paper proposes a novel approach for tuning the primary controller gains and droop coefficients in AC-islanded MGs using

FIGURE 8 | Comparison of the DGs output in parameters change scenario. (a) Frequency, (b) Active power and (c) V_{rms} (pu).

(c) Time(sec)

1.5

0.5

an LMI-based P-LPV-PCA/ H_{∞} control structure. The objective is to regulate the MG frequency considering the nonlinearity and uncertain parameters of the system. The proposed method models all system uncertainties as a P-LPV framework for applying the parameter tuning approach. The PCA algorithm reduces the scheduling parameter size, and the control gains are computed by solving the LMIs defined on the obtained P-LPV model based on H_{∞} performance and stability. The primary

2

2

2

TABLE 4 | The verification of the H_{∞} performance criterion for $\gamma = 1.3$ in loads change scenario.

Item	DG_1	DG_2	DG_3	DG_4
$\frac{ Z_{\infty} _2}{ w _2} < \gamma$	$3.52 \times 10^{-4} <$	$3.55 \times 10^{-4} <$	$3.53 \times 10^{-4} <$	$3.55 \times 10^{-4} <$
$ w _2$	1.3	1.3	1.3	1.3

TABLE 5 | The parameters change scenario.

Description of			
scenarios	$Cf(\mu F)$	$Rf(\Omega)$	Lf (mH)
0 < t < 0.5 (s)	50	0.1	1.35
0.5 < t < 1 (c)	$1.1 \times (50)$	$1.2 \times (0.1)$	$1.2 \times (1.35)$
1 < t < 1.5 (s)	$0.9 \times (50)$	$0.8 \times (0.1)$	$0.8 \times (1.35)$
1.5 < t (s)	50	$0.9 \times (0.1)$	$1.1 \times (1.35)$

control gains and droop coefficients are optimised to minimise the errors between the optimal and actual control signals. The order and structure of the primary control remain unchanged in the proposed approach, making it easy to implement on digital hardware devices of any type. The proposed method is applied to the MG in MATLAB/Simulink, and the simulation results demonstrate the authenticity, effectiveness, and efficiency of the proposed process for MG frequency regulation in the presence of uncertainties, disturbances, nonlinearity, and dynamic changes in MGs. The same strategy may be utilised concurrently in a future study to tune the secondary controller gains.

Nomenclature

C_{fi}, L_{fi}, R_{fi}	The low-pass-filter variables
F_i	The constant term
$I_{ldi}^*,I_{lqi}^*\left(V_{idi}^*,V_{iqi}^*\right)$	The direct-quadrature axis component of the current (voltage) loop input
I_{ldi},I_{lqi}	The component of the output current of the inverter bridge along the direct-quadrature axis.
m_{Pi}, n_{Qi}	The gain of the droop controller
P_i/Q_i	The calculated power (active / reactive) of \mathcal{DG}_i
R_{ci}, L_{ci}	The variables of the output connector
V_{in}	The nominal voltage
V_{odi}^*, V_{oqi}^*	The direct-quadrature axis component of the output of the voltage droop controller
$V_{odi}, V_{oqi}(I_{odi}, I_{oqi})$	The direct-quadrature axis component of the voltage (current) of VSI
ω_b	The nominal angular value
ω_{ci}	The cut-off frequency of low-pass-filter
ω_i	The angular frequency of DG_{i}
ω_{ni}	The nominal angular frequency
$\phi_{di},\phi_{qi},\gamma_{di},\gamma_{qi}$	Supplementary state variables

Author Contributions

Fatemeh Zare-Mirakabad: formal analysis, software and writing – original draft. **Mohammad-Hosein Kazemi:** methodology, supervision, visualisation and writing – original draft. **Aref Doroudi:** validation and writing – review and editing.

Conflicts of Interest

The authors declare no conflicts of interest.

Data Availability Statement

The data are available from the corresponding author upon reasonable request.

References

- 1. X. Xing and L. Jia, "Energy Management in Microgrid and Multi-microgrid," *IET Renewable Power Generation* 18, no. 15 (2024): 3480–3508.
- 2. S. Rogalla, P. Ernst, H. Lens, et al., "Grid-forming Converters in Interconnected Power Systems: Requirements, Testing Aspects, and System Impact," *IET Renewable Power Generation* 18, no. 15 (2024): 3053–3066.
- 3. Y. Zhang, M. Chen, W. Deng, K. Zhong, and Z. Li, "Multi-layer and Timescale Optimal Power Flow Control in Capacitive Coupling Inverter-based Microgrids," *IET Renewable Power Generation* 18, no. 5 (2024): 743–752.
- 4. J. Sharma and T. S. Sidhu, "A Low Voltage Microgrid Protection Scheme Using Digital Instrument Transformers," *IET Renewable Power Generation* 18, no. 6 (2024): 1007–1018.
- 5. A. Najar, H. K. Karegar, and S. Esmaeilbeigi, "Multi-agent Protection Scheme for Microgrid Using Deep Learning," *IET Renewable Power Generation* 18, no. 4 (2024): 663–678.
- 6. M. Y. A. Khan, H. Liu, R. Zhang, Q. Guo, H. Cai, and L. Huang, "A Unified Distributed Hierarchal Control of a Microgrid Operating in Islanded and Grid Connected Modes," *IET Renewable Power Generation* 17, no. 10 (2023): 2489–2511.
- 7. G. Jing, J. Liu, T. Zhao, B. Huang, and R. Wang, "Distributed Dynamic Event-triggered Control for Resilience-oriented Current Sharing in Microgrid," *IET Renewable Power Generation* 18, no. 7 (2024): 1332–1345.
- 8. S. Kanwal, M. Q. Rauf, B. Khan, and G. Mokryani, "Artificial Neural Network Assisted Robust Droop Control of Autonomous Microgrid," *IET Renewable Power Generation* 18, no. 7 (2024): 1346–1369.
- 9. D. Pullaguram, R. Rana, S. Mishra, and N. Senroy, "Fully Distributed Hierarchical Control Strategy for Multi-inverter-based AC Microgrids," *IET Renewable Power Generation* 14, no. 13 (2020): 2468–2476.
- 10. C. Liu, X. Yue, J. Zhang, and K. Shi, "Active Disturbance Rejection Control for Delayed Electromagnetic Docking of Spacecraft in Elliptical Orbits," *IEEE Transactions on Aerospace and Electronic Systems* 58, no. 3 (2021): 2257–2268.
- 11. H. Shayeghi, I. F. Davoudkhani, and N. Bizon, "Robust Self-adaptive Fuzzy Controller for Load-frequency Control of Islanded Airport Microgrids Considering Electric Aircraft Energy Storage and Demand Response," *IET Renewable Power Generation* 18, no. 4 (2024): 616–653.
- 12. A. E. M. Bouzid, P. Sicard, H. Chaoui, and A. Cheriti, "Robust Three Degrees of Freedom Based on $H\infty$ Controller of Voltage/Current Loops

- for DG Unit in Microgrids," IET Power Electronics 12, no. 6 (2019): 1413-1424
- 13. F. Mohammadi, B. Mohammadi-Ivatloo, G. B. Gharehpetian, et al., "Robust Control Strategies for Microgrids: A Review," *IEEE Systems Journal* 16, no. 2 (2022): 2401–2412.
- 14. F. Zare-Mirakabad, M.-H. Kazemi, and A. Doroudi, "Distributed Robust Control of Frequency and Active Power-sharing Ratio Regulation in Islanded AC Microgrids," *Electrical Engineering* 106 (2024): 5909–5918.
- 15. A. Afshari, M. Karrari, H. R. Baghaee, and G. Gharehpetian, "Resilient Synchronization of Voltage/Frequency in AC Microgrids Under Deception Attacks," *IEEE Systems Journal* 15, no. 2 (2020): 2125–2136.
- 16. M. Raeispour, H. Atrianfar, M. Davari, and G. B. Gharehpetian, "Fault-Tolerant, Distributed Control for Emerging, VSC-based, Islanded Microgrids—An Approach Based on Simultaneous Passive Fault Detection," *IEEE Access* 10 (2021): 10995–11010.
- 17. M. Raeispour, H. Atrianfar, H. R. Baghaee, and G. B. Gharehpetian, "Robust Distributed Disturbance-Resilient H_{∞} -Based Control of Off-Grid Microgrids With Uncertain Communications," *IEEE Systems Journal* 15, no. 2 (2020): 2895–2905.
- 18. M. Raeispour, H. Atrianfar, H. R. Baghaee, and G. B. Gharehpetian, "Resilient H_{∞} Consensus-Based Control of Autonomous AC Microgrids With Uncertain Time-Delayed Communications," *IEEE Transactions on Smart Grid* 11, no. 5 (2020): 3871–3884.
- 19. A. B. Farjadian, B. Thomsen, A. M. Annaswamy, and D. D. Woods, "Resilient Flight Control: An Architecture for Human Supervision of Automation," *IEEE Transactions on Control Systems Technology* 29, no. 1 (2020): 29–42.
- 20. M. B. A. Jabali and M. H. Kazemi, "A New LPV Modeling Approach Using PCA-based Parameter Set Mapping to Design a PSS," *Journal of Advanced Research* 8, no. 1 (2017): 23–32.
- 21. M. B. A. Jabali and M. H. Kazemi, "Uncertain Polytopic LPV Modelling of Robot Manipulators and Trajectory Tracking," *International Journal of Control, Automation and Systems* 15 (2017): 883–891.
- 22. S. Azizi, M. H. Asemani, N. Vafamand, S. Mobayen, and A. Fekih, "Adaptive Neural Network Linear Parameter-Varying Control of Shipboard Direct Current Microgrids," *IEEE Access* 10 (2022): 75825–75834.
- 23. S. Jadidi, H. Badihi, and Y. Zhang, "Design of an Intelligent Hybrid Diagnosis Scheme for Cyber-physical PV Systems at the Microgrid Level," *International Journal of Electrical Power and Energy Systems* 150 (2023): 109062.
- 24. N. Vafamand, M. M. Arefi, M. Shafie-Khah, and J. P. Catalão, "Adaptive Optimal Control of Faulty Nonlinear DC Microgrids With Constant Power Loads: Dual-Extended Kalman Filter Approach," *IEEE Transactions on Industry Applications* 59, no. 1 (2022): 513–522.
- 25. G. M. Vinco, O. Sename, G. Strub, and S. Theodoulis, "Linear Parameter-Varying Polytopic Modeling and Control Design for Guided Projectiles," *Journal of Guidance, Control, and Dynamics* 47, no. 3 (2024): 433–447.
- 26. P. Li, A.-T. Nguyen, H. Du, Y. Wang, and H. Zhang, "Polytopic LPV Approaches for Intelligent Automotive Systems: State of the Art and Future Challenges," *Mechanical Systems and Signal Processing* 161 (2021): 107931.
- 27. W. Jiang, C. Zheng, X. Sun, and Y. Wang, "Switching Polytopic Linear Parameter-Varying Control for Hypersonic Vehicles in Full Envelope," *International Journal of Control, Automation and Systems* 22 (2024): 785–796.
- 28. S. Asadi, N. Vafamand, M. Moallem, and T. Dragičević, "Fault Reconstruction of Islanded Nonlinear DC Microgrids: An LPV-Based Sliding Mode Observer Approach," *IEEE Journal of Emerging and Selected Topics in Power Electronics* 9, no. 4 (2020): 4606–4614.
- 29. M. Z. Mansour, M. H. Ravanji, A. Karimi, and B. Bahrani, "Linear Parameter-Varying Control of a Power-Synchronized Grid-Following

- Inverter," IEEE Journal of Emerging and Selected Topics in Power Electronics 10, no. 2 (2022): 2547–2558.
- 30. M. Dehghani, M. Ghiasi, T. Niknam, et al., "Control of lpv Modeled AC-Microgrid Based on Mixed $\rm H_2/H_\infty$ Time-Varying Linear State Feedback and Robust Predictive Algorithm," *IEEE Access* 10 (2021): 3738–3755.
- 31. H. Atoui, O. Sename, V. Milanes, and J.-J. Martinez-Molina, "Toward Switching/Interpolating LPV Control: A Review," *Annual Reviews in Control* 54 (2022): 49–67.
- 32. Y. S. Quan, J. S. Kim, and C. C. Chung, "Linear Parameter Varying Models-based Gain-scheduling Control for Lane Keeping System With Parameter Reduction," *IEEE Transactions on Intelligent Transportation Systems* 23, no. 11 (2022): 20746–20756.
- 33. H. Mohammadi, S. Jokar, M. Mohammadi, A. Kavousi Fard, M. Dabbaghjamanesh, and M. Karimi, "A Deep Learning-to-Learning Based Control System for Renewable Microgrids," *IET Renewable Power Generation* (2023).
- 34. F. Saleem, A. Ali, I.-U.-H. Shaikh, and M. Wasim, "Application and Comparison of Kernel Functions for Linear Parameter Varying Model Approximation of Nonlinear Systems," *Applied Mathematics-A Journal of Chinese Universities* 38, no. 1 (2023): 58–77.
- 35. F. Zare-Mirakabad, M. H. Kazemi, and A. Doroudi, "Robust H_{∞} -Primary Control of AC Islanded Microgrids Based on LPV Modeling," *Iranian Journal of Electrical And Electronic Engineering* 19, no. 3 (2023): 61–73, https://doi.org/10.22068/ijeee.19.3.2724. (in English). Research Paper.
- 36. A. Bidram, F. L. Lewis, and A. Davoudi, "Distributed Control Systems for Small-scale Power Networks: Using Multiagent Cooperative Control Theory," *IEEE Control Systems Magazine* 34, no. 6 (2014): 56–77.
- 37. A. Ghasemi, M. Sedighizadeh, A. Fakharian, and M. R. Nasiri, "Intelligent Voltage and Frequency Control of Islanded Micro-grids Based on Power Fluctuations and Communication System Uncertainty," *International Journal of Electrical Power & Energy Systems* 143 (2022): 108383.
- 38. M. Keshavarz, A. Doroudi, M. H. Kazemi, and N. M. Dehkordi, "A Novel Adaptive Distributed Secondary Voltage Controller With High Convergence Rate for Islanded Microgrids," *IEEE Systems Journal* 15, no. 3 (2020): 4157–4167.
- 39. J. S. Shamma, "An Overview of LPV Systems," in *Control of Linear Parameter Varying Systems With Applications*, eds. J. Mohammadpour and C. Scherer (Springer, 2012), 3–26.
- 40. A. Kwiatkowski and H. Werner, "PCA-based Parameter Set Mappings for LPV Models With Fewer Parameters and Less Overbounding," *IEEE Transactions on Control Systems Technology* 16, no. 4 (2008): 781–788.
- 41. M. H. Kazemi and R. Tarighi, "PID-based Attitude Control of Quadrotor Using Robust Pole Assignment and LPV Modeling," *International Journal of Dynamics and Control* (2024): 1–13.
- 42. A. Fazli and M. H. Kazemi, "Robotic Arm Tracking Control Through Smooth Switching LPV Controller Based on LPV Modeling and Torque Approximation," *Industrial Robot: The International Journal of Robotics Research and Application* 51, no. 2 (2024): 246–257.
- 43. P. P. Khargonekar and M. A. Rotea, "Mixed $\rm H_2/H_\infty$ Control: A Convex Optimization Approach," *IEEE Transactions on Automatic Control* 36, no. 7 (1991): 824–837.
- 44. R. Tarighi, A. H. Mazinan, and M. H. Kazemi, "Integral-based Robust LPV Control of Nonlinear Flight Systems," *Proceedings of the Institution of Mechanical Engineers, Part G: Journal of Aerospace Engineering* 237, no. 4 (2023): 809–823.
- 45. H. Wu and Y. Fei, "Mixed H^2/H^∞ Guaranteed-cost Control for Uncertain Linear Systems," *IFAC Proceedings Volumes* 32, no. 2 (1999): 3508–3513.
- 46. A. Bidram, A. Davoudi, F. L. Lewis, and J. M. Guerrero, "Distributed Cooperative Secondary Control of Microgrids Using Feedback

Linearization," *IEEE Transactions on Power Systems* 28, no. 3 (2013): 3462-3470.

47. D. G. Photovoltaics and E. Storage, "IEEE Standard for Interconnection and Interoperability of Distributed Energy Resources With Associated Electric Power Systems Interfaces," *IEEE Std* 1547 (2018): 1547–2018.

Appendix A

The $A(\mu)$, B_1 , B_2 , and C in Equation (41) are set as follows: